UNIVERSITY OF CALIFORNIA, SAN DIEGO

A Search for New Physics using the $M_{\mathbf{T2}}$ Variable in All-Hadronic Final States produced in proton-proton Collisions with a Center of Mass Energy of 13 TeV

A dissertation submitted in partial satisfaction of the
requirements for the degree
Doctor of Philosophy

in

Physics

by

Mark Derdzinski

Committee in charge:

Professor Frank Würthwein, Chair
Professor Avraham Yagil
Professor Benjamin Grinstein
Professor Farhat Beg
Professor Ian Galton

2018

The dissertation of Mark Derdzinski is approved, and it is acceptable in quality and form for publication on microfilm and electronically:

_____

_____

_____

_____

_____

Chair

University of California, San Diego

2018

DEDICATION

FIXME: Dedication here.

EPIGRAPH

For knowledge comes slowly, and when it comes, it is often at great personal expense.

— Paul Auster, *Ghosts*

TABLE OF CONTENTS

LIST OF FIGURES

LIST OF TABLES

ACKNOWLEDGEMENTS

FIXME: Acknowledgements

VITA

2011	B. A. in Physics and Mathematics, University of California, Berkeley
2014	M. S. in Physics, University of California, San Diego
2018	Ph. D. in Physics, University of California, San Diego

PUBLICATIONS

Search for new physics with the M_{T2} variable in all-jets final states produced in pp collisions at $\sqrt{s} = 13$ TeV, *The CMS collaboration, Khachatryan, V., Sirunyan, A.M. et al.* J. High Energ. Phys. (2016) 2016: 6. doi:10.1007/JHEP10(2016)006 `arXiv:1603.04053 [hep-ex]`

Search for new physics in the one soft lepton final state using 2015 data at $\sqrt{s} = 13$ TeV, *CMS Collaboration*, Physics Analysis Summary (2016), CMS-PAS-SUS-16-011

FIXME: Add 2017 MT2 paper citation

ABSTRACT OF THE DISSERTATION

A Search for New Physics using the $M_{\mathbf{T2}}$ Variable in All-Hadronic Final States produced in proton-proton Collisions with a Center of Mass Energy of 13 TeV

by

Mark Derdzinski

Doctor of Philosophy in Physics

University of California, San Diego, 2018

Professor Frank Würthwein, Chair

FIXME: Add Abstract.

Chapter 1

Introduction

1.1 The Standard Model of Particle Physics

1.2 Issues with the Standard Model

1.3 Beyond Standard Model Physics

Chapter 2

The Large Hadron Collider and the CMS Detector

2.1 The Large Hadron Collider

FIXME: add paragraphs on LHC

2.2 The Compact Muon Solenoid

The Compact Muon Solenoid (CMS) is a general-purpose physics detector at the LHC, situated at one of the five collision points along the main ring. The detector encapsulates the collision point with layers of various subsystems designed to interact with the outgoing particles of the proton-proton collisions, and measure the position and energies of the collision products. Because of the extremely high rate of interactions at the collision

point (on the order of one billion interactions per second), saving data from every bunch crossing would be unsustainable, and so the detector is also equipped with a system of hardware and software implemented "triggers" which identify events of interest for physics analyses to be saved to disk for further analysis.

The physical construction of the detector is motivated by the different interaction of particles with different types of materials, and consists of several subsystems layered as coaxial cylinders around the interaction point. Each subsystem consists of (sometimes different) components covering the fiducial area coaxial with the beamline (the "barrel") and also the ends of the cylinder (the "endcaps"). The innermost subsystem of CMS is the silicon tracker, which consists of many layered silicon pixels designed to pinpoint the locations of charged particles while minimally interacting with the particle's trajectory. The layer beyond the tracker is the electromagnetic calorimeter (ECAL), a grid of lead-tungstate crystals which scintillate to measure the energies of electromagnetic particles. Beyond the ECAL is the hadronic calorimeter (HCAL), a sampling calorimeter designed to measure the energies of hadronic particles (which deposit minimal energy in the ECAL). The final, outer layer is the CMS muon detector, where the muon detection stations are interweaved with the magnetic return yoke that generates the toroidal 3.8T magnetic field inside the detector volume. The total dimensions of the detector are **FIXME: cms actual size**.

2.2.1 Silicon Tracker

The silicon vertex tracker (SVT) is a series of silicon pixels and strips designed to measure the position of charged particles in the detector, while disturbing their path as little as possible. The position of particles in the interior is of particular importance in event reconstruction; charged particles traveling in a magnetic field will deflect in a curved path with radius proportional to the particles momentum as described in equation 2.1, and so the track reconstruct can be used to not only determine a particle's momentum with high precision, but also the sign of its charge based on the direction of curvature.

$$p = qrB \tag{2.1}$$

As the innermost detector subsystem, the SVT experiences the highest flux of particle radiation. In the barrel region, the tracker layers are oriented in 3 coaxial layers. Closest to the interaction point where particle flux is the greatest, very precise silicon pixels are used, measuring $100 \times 150 \mu\text{m}^2$, whereas in other layers the flux is low enough to use microstrip detectors, measuring $10\text{cm} \times 80\mu\text{m}$ and $25\text{cm} \times 180\mu\text{m}$ in the middle and outer layers respectively. In the endcaps, the pixel strips are arranged in a turbine-like pattern in two separate layers on each end. This configuration allows for the precise measurement of particle position for track reconstruction, while minimizing the amount of material which might deflect particles from their original trajectories. A partial geometry of the SVT layout can be seen in figure 2.1.

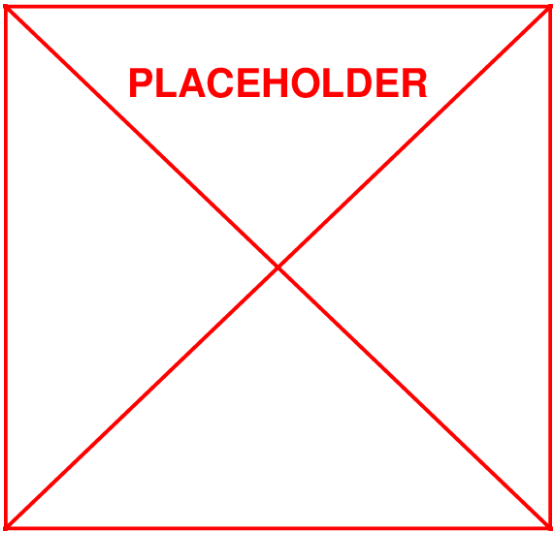

Figure 2.1: Geometry of silicon tracker inner layers in CMS.

2.2.2 Electromagnetic Calorimeter

The ECAL is used to measure the energies of particles which interact electromagnetically, both absorbing the incident particles and scintillating to provide an energy-readout to photodiodes attached to each crystal. Constructed of lead-tungstate ($PbWO_4$), electromagnetically interacting particles (such as electrons or photons) will interact with the crystal material, losing energy through a cascade of electromagnetic interactions including election-positron pair production and bremsstrahlung, as pictured in figure 2.2. This phenomenon — also referred to as "showering" — causes the crystals to scintillate proportional to the energy deposited in the crystal, which is then measured by various photodiodes to extract an accurate measurement of the particle energy, now fully absorbed by the calorimeter.

The fundamental principle of the calorimeter measurement relies on the energy loss

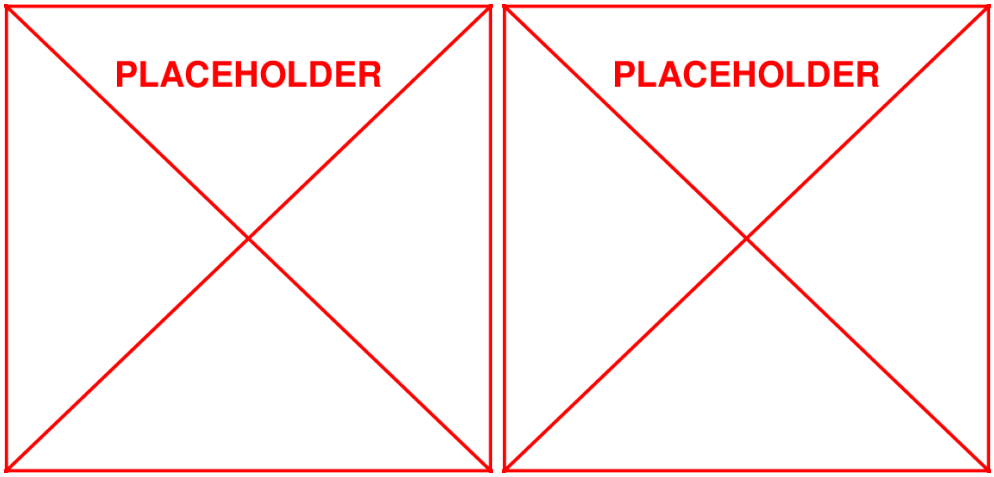

Figure 2.2: Feynman diagrams depicting the main processes by which particles shower in the ECAL. The left diagram depicts electron-positron pair production from a photon, and the right diagram depicts bremsstrahlung, where an electron radiates energy away through a photon.

of particles interacting with matter. In general, the energy of a particle traveling a distance X through some material is given by equation 2.2, where E_0 is the initial energy of the particle and X_0 is the material-dependent radiation length.

$$E(x) = E_0 e^{\frac{-x}{X_0}} \tag{2.2}$$

The design of the calorimeter is motivated by the choice of a scintillating, radiation-hard material with short X_0 such that incident electromagnetic particles deposit all their energy and are stopped by the ECAL. The resolution of the energy measurement is also dependent on the "stochastic term", which parametrizes the uncertainty due to statistical and measurement fluctuations in the calorimeter, and is given by equation 2.3, where S is

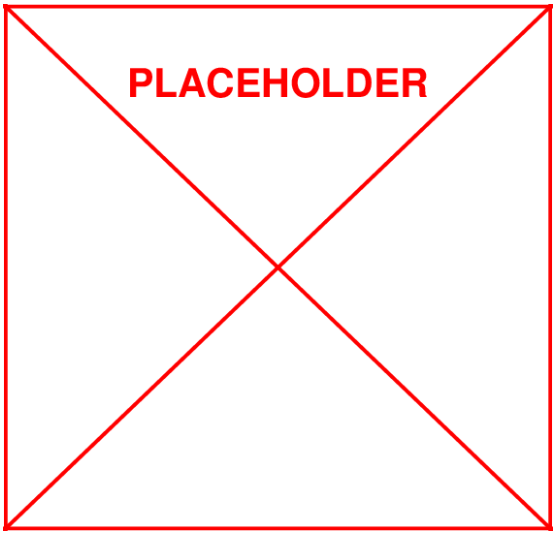

Figure 2.3: Energy resolution σ/E of the ECAL as a function of electron energy measured using a test beam. The energy was measured in a 3×3 crystal array with electrons incident on the center crystal, with electrons falling in a $4 \times 4\text{mm}^2$ region (lower points) and $20 \times 20\text{mm}^2$ region (upper points).

the stochastic term, N the noise, and C the constant term.

$$\left(\frac{\sigma}{E}\right)^2 = \left(\frac{S}{\sqrt{E}}\right)^2 + \left(\frac{N}{E}\right)^2 + C^2 \tag{2.3}$$

The energy resolution can be measured by a test beam of known energy, as shown in figure 2.3.

The construction of the calorimeter is also divided into two sections by the cylindrical geometry, the ECAL barrel section (EB) and ECAL endcap sections (EE). The EB consists of 61,200 crystals arranged into 36 "supermodules", each spanning half the barrel length, and uses silicon avalanche photodiodes (APDs) as photodetectors. The individual crystals are tilted slightly (3°) in an $\eta - \phi$ grid with respect to the nominal interaction

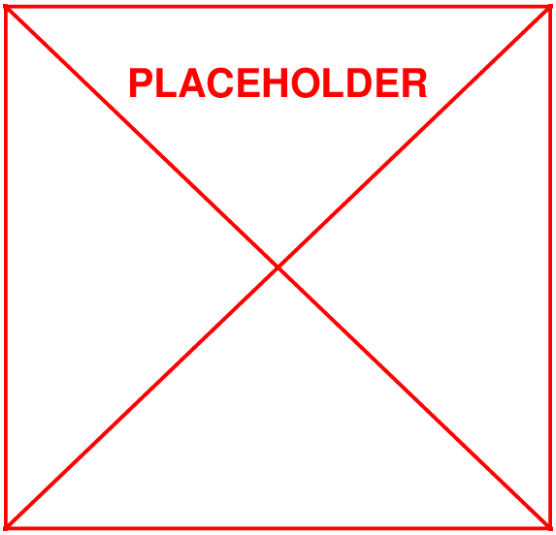

Figure 2.4: A cross section of the ECAL geometry, with the dashed lines marking the pseudorapidity values η covered by the various subsystems.

point, with a front-facing area of $22 \times 22\text{mm}^2$ and a length of 230mm. The EE instead uses vacuum phototriodes (VPTs) as photodetectors, and consists of approximately 15,000 crystals clustered in 5×5 units, also offset from the interaction point but arranged in an $x-y$ grid, with a cross section of $28.6 \times 28.6\text{mm}^2$ and a length of 220mm. The EE is also equipped with a "preshower" device placed in front of the crystal calorimeter, consisting of two strips of silicon strip detectors to enhance π^0 rejection. The layout of the ECAL can be seen in figure 2.4. Because of the depth of the ECAL crystals (which are $\sim 25X_0$, and the confining properties of the crystals (which have a Moliere radius of 2.2cm, the radius of a cylinder containing 90% of a shower's energy on average), electrons and photons are typically well reconstructed in CMS, except in the transition region where EB and EE meet.

2.2.3 Hadronic Calorimeter

The CMS HCAL is a sampling calorimeter. Designed with alternating layers of scintillating and absorbing material, incident hadronic particles (such as charged pions, kaons, protons, etc.) interact with the absorber material and consequently shower into electromagnetic particles, whose energy can be read out by photodiodes connected to the scintillating material. Brass is used as the absorber material for both its interaction length and non-magnetic properties, and plastic scintillator tiles connected to embedded wavelength-shifting fibers carry the light to a readout system.

As with the ECAL, the energy loss of hadronic particles in the absorber is characterized by the (hadronic) interaction length and equation 2.2. However, unlike the ECAL, the HCAL contains both hadronic and electromagnetic showers. Electromagnetic particles generated in hadronic showers often fail to escape the absorber layers, and thus some electromagnetic energy is lost in the absorbers. The CMS HCAL is sometimes referred to as a *non-compensating calorimeter* because it is not constructed to actively compensate for the energy lost to these electromagnetic effects and the energy measurements must be corrected offline, known as "jet energy corrections" (JECs). JECs are typically calculated by examining data from collisions producing a photon recoiling against hadronic particles. By accurately measuring the photon energy in the ECAL, the sum of the recoiling hadronic energy in the HCAL is inferred (by momentum conservation) and compared to the detector response. Because the performance of the HCAL can fluctuate with time and run conditions, JECs are regularly recalculated and applied to the raw energy measure-

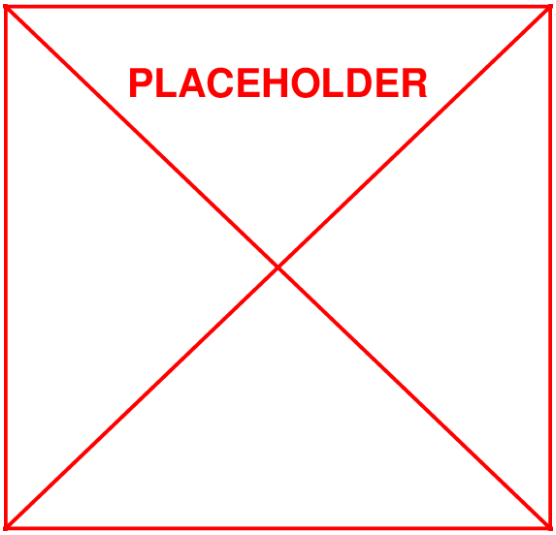

Figure 2.5: The jet transverse energy resolution as a function of the jet transverse energy, in different regions of pseudorapidity. For an explanation of jets, see section 2.3.4

ments taken by the HCAL to compensate for these effects. The energy resolution of the HCAL in different regions of pseudorapidity can be seen in figure 2.5.

The geometry of the HCAL can be reduced to four sections. The HCAL barrel (HB) consist of 32 "towers" of alternating absorber/scintillator material spanning the pseudorapidity region $-1.4 < \eta < 1.4$. The HCAL outer (HO) detector lies outside the vacuum tank of the magnetic coil and measures energy from any hadronic particles "leaking" through the HB, covering the pseudorapidity region $-1.26 < \eta < 1.26$. The HCAL endcap (HE) consists of 14 η towers spanning the pseudorapidity range $1.3 < |\eta| < 3.0$. Finally, the HCAL forward (HF) is a different steel/quartz fibre calorimeter spanning the very-forward $3.0 < |\eta| < 5.0$ region. Instead utilizing Cherenkov radiation generated in the quartz fibers, the HF preferentially samples neutral hadronic energy and is ideally designed for the hadronic-heavy radiation environment in the forward region.

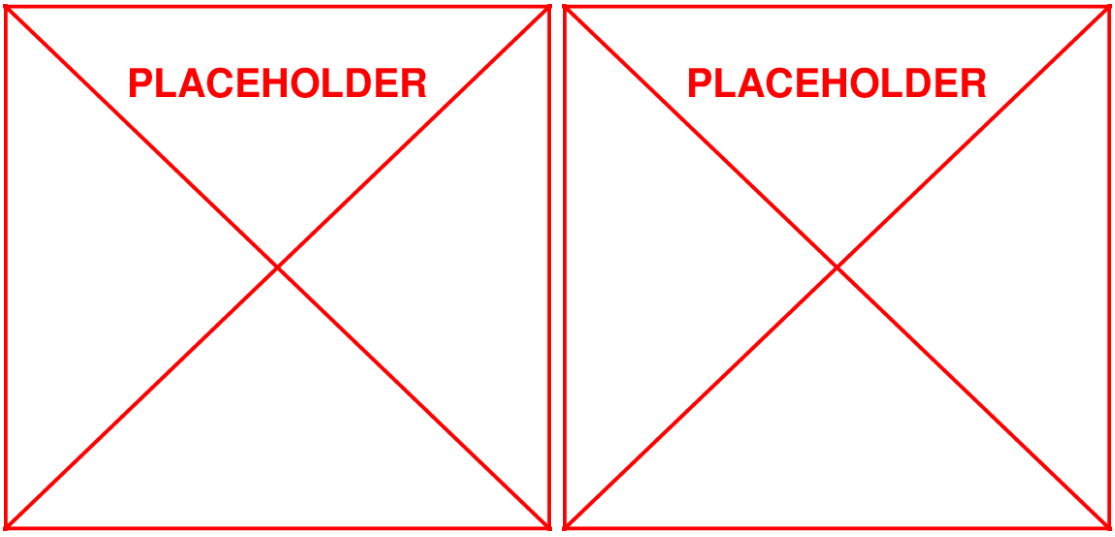

Figure 2.6: Muon momentum resolution as a function of muon momentum using only the inner tracking system, only the muon system, or both combined in the barrel region (left) or endcap region (right).

2.2.4 Muon Detectors

The muon detector is the only subsystem which is constructed outside of the toroidal magnetic field. Interleaved with the magnetic return yoke, different muon detectors are used to aid in the identification and reconstruction of muon tracks. Because muons typically penetrate every other layer of the detector and have a large bending radius, additional measurements in the muon system — combined with measurements in the SVT — can lead to vastly improved resolution of muon momentum. The non-uniform magnetic field in the muon detector region (beyond the toroidal regime) causes an s-shaped trajectory and tighter bending radius (than in the SVT) for the muons, which improves the resolution for particles with transverse momentum above ~ 200GeV as seen in figure 2.6.

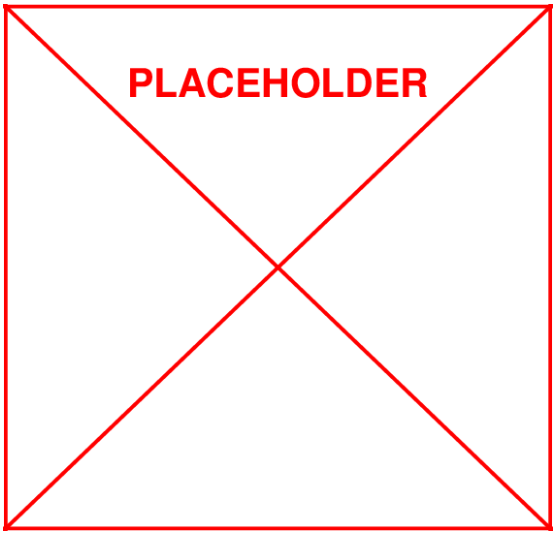

Figure 2.7: Layout of the CMS muon system for initial run configurations. The DT system is used only in the barrel region and CSCs in the endcap region, while RPCs are deployed in both the barrel and endcap.

Different types of muon detectors are deployed (sometimes in combination) in different sections of the full muon system. In the barrel region ($-1.2 < \eta < 1.2$) where the muon flux, neutral background, and magnetic field are small, drift tube (DT) chambers are used. In the endcaps where the the muon flux, neutral background, and magnetic field are much greater, cathode strip chambers (CSC) are used to increase coverage up to $|\eta| < 2.4$. In addition to these technologies, both the barrel and endcap systems are supplemented with resistive plate chambers (RPC) to provide complementary information to the DT and CSC detectors. The layout of the different muon detector components in the barrel and endcap can be seen in figure 2.7.

The DT detectors are chambers filled with gas surrounding a wire, with a voltage difference between the wire and outside of the DT. When charged particles pass through

the drift chamber, they ionize the gas, and the ionization products will drift across the voltage difference in the tube, resulting in a detectable voltage change in the DT. By measuring both the position along the DT wire where charge is deposited, as well as reconstructing the "drift time" it takes for the ionized particles to reach the wire, DTs provide a 2-dimensional measurement of a particle's position. In CMS, the DT chambers consist of a dozen layers arranged into 3 groups, each with up to 60 DTs. The layers are arranged in such a way that some measure the direction of the muon parallel to the proton beam and others along the perpendicular coordinate, such that the full muon trajectory can be reconstructed by using the DT station information.

FIXME: add paragraph on CSCs

FIXME: add paragraph on RPCs

2.2.5 Trigger Systems

When operating at design luminosity, the LHC can deliver proton bunches to the collision point at a rate of 40MHz (or 25ns between bunches), resulting in an average collision rate on the order of one billion collisions per second. In order to achieve reasonable rates of data collection for offline storage and processing, the detector must suppress the event rate by six orders of magnitude when selecting events of interest to be saved for physics analyses. This is accomplished through a combination of readout electronics and the trigger systems: the Level-1 trigger (L1) processors and online High-Level triggers (HLT).

The L1 trigger system is comprised of specialized hardware processors to rapidly

pre-select events of interest based on the calorimeter and muon systems. Based on the beam crossing frequency, the L1 electronics have only a few microseconds to collect readout data from the front end electronics and execute logic to select events of interest, such that the total time allotted for L1 trigger calculations is $< 1\mu s$. During this time the bulk of detector data is held in a buffer while L1 trigger decisions are made based on data with reduced granularity and resolution rapidly collected from the calorimeter and muon systems, where triggers typically check for "trigger primitive" objects (such as photons, muons, electrons, etc.). Trigger primitives must meet certain momentum or energy thresholds, and L1 triggers may also check global data about the event such as the sum of transverse energy or the missing transverse energy (inferred from momentum conservation).

After an L1 trigger tags an event, high-resolution data is read out from buffers for additional data processing before reaching the HLT. Each event of $\sim 1.5MB$ is transferred to front-end readout buffers which then pipes data to a processor containing the HLT code. HLT code is designed to discard events as soon as possible when making trigger decisions and only a subset of objects or partial reconstruction of events may occur before the final trigger decision is made, though HLT algorithms typically approach the quality of final reconstruction. The HLT reduces the L1 output rate to $\mathcal{O}(100\text{Hz})$ for event storage and full reconstruction.

2.3 CMS Physics Objects

When physics events are fully reconstructed, detector data is used to identify *physics objects* representing real particles and event quantities for use in a physics analysis. The physics objects in an event — such as leptons, jets, or missing energy — and their properties are used to select events of interest for physics analyses targeting different final states. The properties of physics objects and global event data are also be used to make analysis level decisions of the quality of different objects. Here we describe some of the physics objects referred to in this analysis and how they are reconstructed, as well as some global event properties and quality variables used as discriminants for physics objects and events.

2.3.1 Particle Flow

Most of the physics objects described in the following sections are reconstructed and identified in CMS using the particle flow (PF) algorithm. The PF algorithm is a holistic, iterative algorithm which uses all the available data in the detector to classify "PF candidate" particles in an event. PF works iteratively by identifying tracks and calorimeter deposits into a PF candidate, removing all energy and hits associated with the candidate and repeating the algorithm until all the detector information has been associated to PF objects. First any muon tracks in the inner tracker associated with muon system hits are associated and removed. remaining tracks are extrapolated into the calorimeters, and any energy deposits on the path are associated with the track and removed from further consideration. Once all the tracks have been associated, the remaining energy clusters can

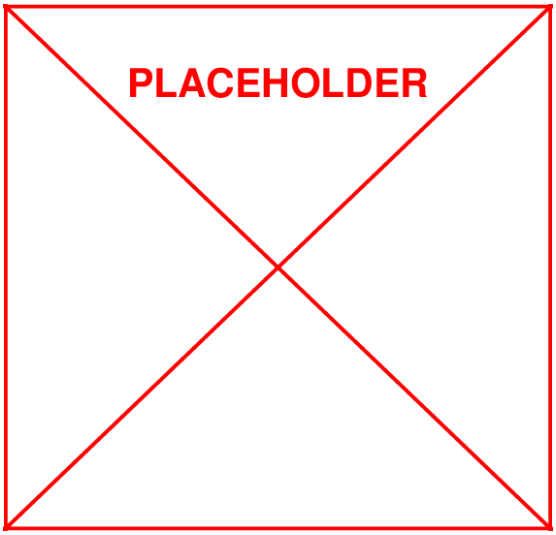

Figure 2.8: A graphic depiction of different particles leaving various signatures in the different CMS detector subsystems. Particles may be detected via tracks hits, energy deposits, or a combination of both.

be identified with photons and neutral hadrons (depending on their presence in the ECAL or HCAL, respectively). An example of the different tracks and energy deposits associated with various particles can be seen in figure 2.8.

2.3.2 Isolation

2.3.3 Leptons and Photons

2.3.4 Jets

2.3.5 Missing Energy

Chapter 3

The $M_{\mathbf{T2}}$ Variable Search

3.1 Analysis Strategy

Searches for new physics targeting all-hadronic final states present unique challenges and opportunities at the LHC. While such searches typically implement stringent vetoes on lepton candidates and thus bypass the need to correctly identify "real" leptons from similar signals in the detector, the high rate of QCD processes in proton-proton collisions generates large amounts of SM events (with all-hadronic final states). Designing a search targeting signatures with all-hadronic final states thus requires a mechanism to distinguish and suppress the selection of SM-QCD events from new physics signatures, as well as robust background estimation methods to predict the yield of standard model events which may generate a momentum imbalance in the detector reconstruction of the event (such as $Z \to \nu\nu$).

The M_{T2} analysis harnesses the discriminating power of the M_{T2} stransverse mass

variable to distinguish standard model events from possible signatures including new physics. By first requiring a nominal amount of missing energy in the event, SM-QCD processes are greatly suppressed (since missing energy is not due to physics processes but detector reconstruction or mis-measurement of the underlying event). Additional requirements on the topology of the event (implemented using M_{T2}) further suppress QCD-like processes and favor events with real missing energy anti-aligned with the all-hadronic energy deposits in the detector. After estimating the minimal QCD contribution remaining by extrapolating from a region orthogonal to the signal selection, the only remaining backgrounds are leptonic events where the lepton was failed to be constructed or identified (or "lost-lepton" events), and SM events where energy escapes the detector in the form of neutrinos from a decaying Z boson recoiling against jets (or "invisible Z" events).

3.2 The M_{T2} Variable

3.3 Event Selection Criteria

The general strategy for the event selection is to first apply baseline cuts on motivated by hardware and software-level triggers **FIXME: call back to trigger section in previous chapter? or explain triggers** and reducing the QCD multi-jet background to negligible levels. Events are further categorized using the scalar sum of the transverse momenta p_{T} of all selected jets (H_{T}), the total number of jets in the event (N_{jets}), the total number of b-tagged jets in the event ($N_{\mathrm{b\text{-}jets}}$), and M_{T2} . Events are reconstructed

with the CMS particle-flow (PF) algorithm **FIXME: cite PF**, which is designed to holistically use all event information from each detector element to reconstruct and identify each particle in the event (hereafter referred to as "PF candidates"). A summary of the event preselections can be found in **FIXME: cite table with preselections**.

3.4 Search Regions

3.5 Control Regions

Chapter 4

Background Estimates

4.1 Types of Backgrounds

4.2 Multi-jet Estimate

4.3 Lost Lepton Estimate

4.4 Invisible Z Estimate

Chapter 5

Results

5.1 Yields and Significances

5.2 Signal Interpretations

Chapter 6

Naturalness and Soft Leptons

6.1 Natural Supersymmetry

6.2 Extending the $M_{\mathbf{T2}}$ Search

6.3 Searching for Natural Susy with Soft Leptons

Bibliography